

Numerical study of magneto-convection flows in a complex prototypical liquid-metal fusion blanket geometry

Yi Yan*, Alice Ying, Mohamed Abdou

Mechanical and Aerospace Engineering Department, UCLA, Los Angeles, CA, USA



ARTICLE INFO

Keywords:
Magnetohydrodynamics(MHD)
Magneto-convection
WCLL blanket
Fusion relevant condition
COMSOL multiphysics

ABSTRACT

Numerical simulation of time-dependent magneto-convection flows in a liquid metal breeding blanket unit cell prototypical to the geometry of Water-Cooled Lithium-Lead (WCLL) breeding blanket is performed by COMSOL Multiphysics. Its modeling capability for fully coupled magnetohydrodynamic (MHD)/heat transfer flows in a complex geometry under fusion relevant conditions is tested with the demonstration of the main flow features and temperature profiles. Here, the magneto-convection flow in the bulk region is dominated by the effect of natural convection, leading to two columnar-like, counter-rotating circulations which occupy the whole plenum region of the breeding zone along the external magnetic field direction. High velocity flow jets with the magnitude of 1–2 orders greater than inlet velocity are formed near structural walls that are parallel to the applied magnetic field and break into unsteady sidewall vortices that are mainly confined in boundary layers. Due to the buoyancy effect, the hot fluid particles are stratified near the top structure wall where the cooling effect is the least. The calculated maximum temperature at the wall is lower than the structure's temperature limit but still exceeds the corrosion temperature limit.

1. Introduction

In liquid metal (LM) breeding blanket concepts for fusion power reactors, the breeder material always consists of lithium or lithium-containing alloy as lithium is required for breeding tritium, the indispensable reactant to produce self-sustaining fusion reaction. PbLi is an attractive candidate as lead serves as a neutron multiplier in corresponding nuclear reactions. Electrically conducting flow of LM, such as PbLi, will experience strong magnetohydrodynamic (MHD) effects in the presence of the strong plasma-confining magnetic field, leading to several crucial issues for all LM blanket concepts [1]. Besides the MHD effects, the flowing liquid metals in blanket conduits will experience strong buoyancy forces associated with high temperature gradients due to steep volumetric heat loads and/or surface heating. The interaction between MHD and buoyancy forces, known as magneto-convection, could dominate the flow phenomena and impact the feasibility of most fusion LM blanket designs. Moreover, the flow behaviors, and heat and mass transfer associated with magneto-convection effect will strongly depend on the geometry of specific blanket concepts.

Water-Cooled Lithium-Lead (WCLL) breeding blanket is the most promising liquid breeder blanket concept for DEMO in the EUROfusion Work Package Breeding Blanket (WPBB) – 2018. It is composed of 16 sectors, each of which contains two inboard and three outboard Single

Module Segments (SMS) [2,3]. In the present work, the WCLL module in equatorial outboard (Fig. 1) is considered as the reference computational geometry to study magneto-convection flow behaviors under its fusion relevant conditions. This outboard breeding module contains two identical breeding cells staggered on each other in the poloidal direction as shown in Fig. 2. For each breeding cell, five poloidal plates and one long toroidal plate are inserted to stiffen the breeding zone, separating six rectangular ducts that connect to inlet and outlet manifolds respectively, and leaving the breeding zone open (here named as the plenum region) from the first wall to the edge of stiffening plates. Cooling water, at an operating range of temperature from 295 °C to 328 °C and pressure of 155 bar [4], is used to extract the heat through the circular pipes immersed in the breeding zone. Those components in WCLL introduce significant geometrical complexity that makes it difficult to predict MHD/heat transfer flow via numerical simulations.

Few studies have been conducted for steady-state MHD flow and heat transfer in simplified model geometry of WCLL blankets. To predict the flow behavior in inlet/outlet ducts with streamline cooling pipes immersed in WCLL blanket, Bühler and Mistrangelo [5] simulated fully developed LM flow, driven by either pressure or buoyancy force, in a square duct with one cooling pipe inserted at the duct center. Tassone et al. [6] evaluated and analyzed heat transfer and the performance of water-cooling system in the PbLi plenum region in an

* Corresponding author.

E-mail address: yiyan@fusion.ucla.edu (Y. Yan).

infinite, long squared duct with U-shape water pipes mounted on one sidewall. Both studies showcase the effects of adding cooling pipes into MHD duct flows; however, the actual velocity and temperature distributions, and temporal evolution of MHD flows in prototypical WCLL blanket design have not yet been obtained. The purposes of the present study are to 1) evaluate the modeling capability of COMSOL Multiphysics for time-dependent MHD/heat transfer flows in complex geometry, and to 2) reveal and expose the flow behavior and heat transfer phenomena in the WCLL prototypical blanket design under fusion relevant conditions.

2. Problem formulation

The computational domain in this study consists of one breeding cell but with only half of the cell in the toroidal direction due to geometrical symmetry. Moreover, due to the availability of the in-house computational capability, the breeding cell is further reduced. The final simulation geometry (Fig. 3) is made from the following four simplifying reductions of the original blanket cell (Fig. 1).

- a Only one of the two identical breeding cells stacked in poloidal direction is simulated. Simulating one of them is sufficient because, while electrical couplings do exist on the wall interface between those two cells, the effect of such interactions is still captured via special treatment (i.e. periodic boundary condition).
- b A symmetry condition is used to halve the geometry since all components in the WCLL blanket module (Fig. 1) are symmetric with respect to the center poloidal-radial plane. The cooling effect from water pipes in the breeding zone coolant is also symmetric to the center plane.
- c First wall geometry with embedded cooling pipes is removed from the original module cell. Instead, uniform negative surface heat flux (heat sink) is applied to represent the resultant cooling effect, which closely approximates to be symmetric to the center plane although the flow of water coolant in the first wall is technically asymmetric.
- d To accommodate in-house, current computational hardware capability, about a length of 20 cm of inlet/outlet ducts formed by stiffening plates is removed from the original blanket cell. This should not affect the PbLi flow behavior in the plenum region because the development length of MHD duct flow is expected to be relatively short in the presence of a strong transverse magnetic field [7].

Some of the geometrical parameters are marked in Fig.3 on both the side view and the front view of the computational domain, and their values are listed in Table 1.

The magneto-convection flow of the present study is governed by the combination of incompressible Navier-Stokes equations with Boussinesq's approximation, Ohm's law and electrical current continuity equation, as well as the energy equation. The dimensional form

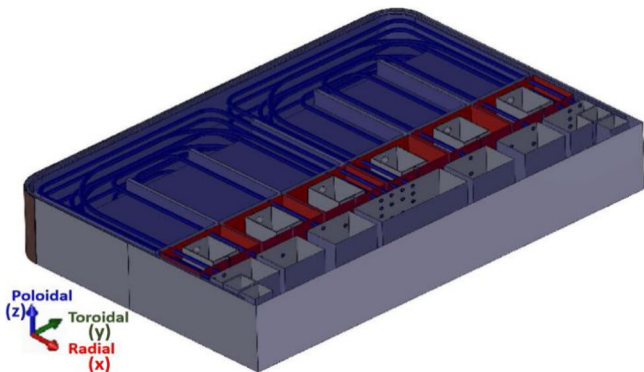


Fig. 1. WCLL equatorial outboard module cell [13].

of these governing equations is written below.

$$\nabla \cdot (\mathbf{u}) = 0 \quad (1)$$

$$\rho \frac{\partial \mathbf{u}}{\partial t} + \rho (\mathbf{u} \cdot \nabla) \mathbf{u} = -\nabla p + \mu \nabla^2 \mathbf{u} + \mathbf{J} \times \mathbf{B} + \rho \mathbf{g} (1 - \beta (T - T_0)) \quad (2)$$

$$\nabla \cdot \mathbf{J} = 0 \quad (3)$$

$$\mathbf{J} = \sigma (-\nabla \phi) + \sigma (\mathbf{u} \times \mathbf{B}) \quad (4)$$

$$\rho C_p \frac{\partial T}{\partial t} + \rho C_p (\mathbf{u} \cdot \nabla) T = \kappa \nabla^2 T + q_v \quad (5)$$

Here, \mathbf{u} , p , and T are the computational variables of the velocity field, pressure, and temperature that are solved for the fluid domain, while the variable of electrical potential (ϕ) is calculated on the entire domain of fluid, coolant pipe and structural walls. The physical properties used in this simulation are that of liquid breeder (PbLi) and structure wall (EUROFER 97 steel) evaluated at the temperature of 710 K (the midpoint in PbLi operation range from 597 K to 823 K [4]) and are listed in Table 2 and Table 3 respectively.

3. Numerical modeling

COMSOL Multiphysics is utilized to study the fully coupled MHD/heat transfer flows in a WCLL breeding cell as described in Section 2. The modeling capability of COMSOL Multiphysics for isothermal MHD flows has been validated by Sahu and Bhattacharyay [11] and Yan [12]. The extended capability of modeling MHD/heat transfer flows in simple geometries has also been validated against various experimental data and numerical results by the author of this paper with the workpieces in progress and under review.

3.1. Mesh processes

A hybrid mesh (Fig. 4) consisting of a combination of non-uniform parallelepiped, triangular prism, and free tetrahedral geometry is applied to the computational domain. To assess the mesh-sensitivity of a solution, the sufficiency of spatial resolution in boundary layers was evaluated as the first step from the solutions of a fully developed MHD flow applied to the geometry of the inlet 1 surface as shown in Fig. 3 (similar to geometry in the study performed by Bühler and Mistrangelo [5]). The calculated electrical potential and the streamlines of electrical current density plotted in Fig. 5 reflect the existence of internal boundary layers near the water pipes, which is an indispensable feature for MHD flow in a duct with immersed pipes [5]. Pressure drop, and maximum velocity quantities are compared among different mesh cases summarized in Table 4, from which case #3 shows insignificant change with continuously compacted mesh. The element sizes corresponding to case #3 on boundary layers (Table 4) are 0.016 mm, and 0.14 mm near the Hartmann walls, and sidewalls, respectively.

The next step in the mesh sensitivity study was to conduct 3D MHD/heat transfer simulations with different mesh resolutions in the bulk region of the breeding zone with free tetrahedral elements while satisfying the requirement of resolution in the boundary layers as established in this step. In particular, the tetrahedral elements meshed in the bulk region, that are determined by the three parameters listed in Table 5, are examined and discussed in Section 4.1. In Table 5, the smallest element size in the bulk region is 3.73 mm in the case of fine mesh, which is the one where the present results were based on. To overcome a large growth rate in element size from the thin boundary layers to the bulk region, four stretching layers were inserted in between. The mesh study concluded with the first layer thickness of δ_{Ha} , δ_{Side} (defined in Table 4) and their subsequent sizes increase by 20 % from one layer to the next. As a result, the element sizes in those transitional regions next to the bulk region are 0.53 mm and 6.1 mm in the vicinity of Hartmann walls and sidewalls respectively.

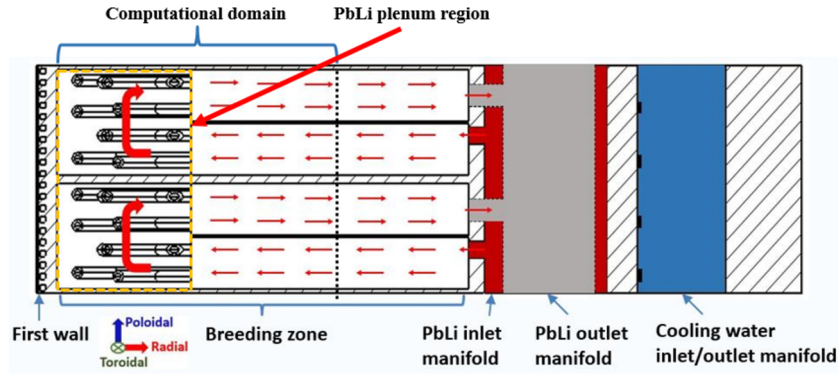


Fig. 2. Section view on poloidal-radial plane of WCLL equatorial outboard module cell [13] with PbLi flow path demonstration (dash line is the reference for computational geometry described in next section).

3.2. Inlet/outlet and boundary conditions

Being relevant to fusion WCLL operational conditions [4,6,8], the input parameters and boundary conditions in this numerical modeling are listed in Table 6 and Table 7 respectively. Due to the fact that the decreased nuclear heating power (Eq. (6)) in WCLL blanket [13] at the end of the simulation domain is still nontrivial in this study (since in this simulation the radial length of the WCLL unit cell has been cut out to overcome the insufficient computational hardware capability), the gradient of velocity deduced from the buoyancy force normal to the outlets would be inconsistent with the boundary condition there. To eliminate this conflict, the nuclear heating profile in this study is ramped down by multiplying a smoothed Heaviside function (Eq. (7)) [14] from the unity to zero value at the last 10 cm from the outlets. Since our interest was to discover the MHD/heat transfer phenomena in the plenum region and it should not be affected as the heating profiles in that region are prototypical to the WCLL nuclear heating profiles as shown in Fig. 6. Such modification should also not hinder our evaluation of this numerical code's capability-as one of the objects of this work. In Table 7, the effective thermal conductance on the interface between PbLi and cooling pipes (CP) is calculated from the thermal resistance circuit theory as $h_{PbLi/CP} = (1/h_{CP} + 1/h_{water})^{-1} = 3480 \text{ W/m}^2\text{K}$, where $h_{CP} = 2\kappa_{wall}/d_i \ln(d_o/d_i)$, and h_{water} is evaluated from Dittus-Boelter Correlation [15].

$$q_V(x) = \begin{cases} -98.962x + 9.5968, & 0 < x < 0.05 \text{ (m)} \\ 365.35x^4 + 443.1x^3 + 215x^2 + 54.376x + 6.8831, & 0.05 \text{ (m)} \leq x \leq L \end{cases} \quad (6)$$

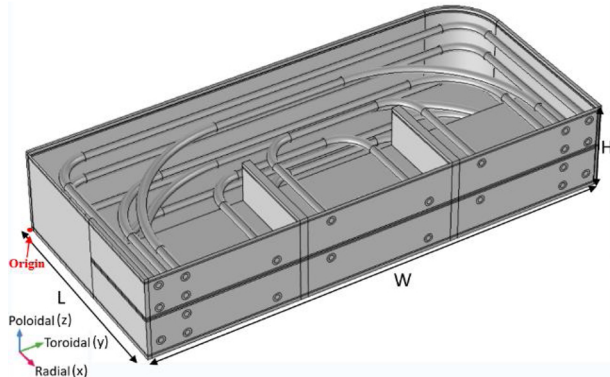


Table 1

Computational WCLL blanket geometry parameters, length in (mm) [8].

Parameter (Symbol)	Value	Parameter (Symbol)	Value
Radial length (L)	330	Inlet/outlet 1 width (b1)	231
Toroidal length (W)	731	Inlet/outlet 2 width (b2)	231
Poloidal length (H)	135	Inlet/outlet 3 width (b3)	233
Water pipe ID (d_i)	8	Inlet/outlet height (a)	61.5
Water pipe OD (d_o)	13	Breeder zone Inlet/outlet length (Ld)	150
Wall thickness (δ)	3	PbLi plenum length (Lp)	174

Table 2

PbLi physical properties, evaluated at $T_{ref} = 710\text{K}$ [9].

Parameter (symbol)	Unit	Value
Density (ρ)	kg/m ³	9672
Dynamic viscosity (μ)	Pa*s	1.343×10^{-3}
Thermal conductivity (κ)	W/(m*K)	15.80
Specific heat (c_p)	J/(kg*K)	188.5
Thermal expansion coeff. (β)	1/K	1.230×10^{-4}
Electrical conductivity (σ)*	S/m	7.562×10^5

* In reference [9] used in Table 2, the unit of electric resistivity of PbLi should be $\Omega \cdot \text{cm}$ instead of $\Omega \cdot \text{m}$.

Table 3

EUROFER97 physical properties, evaluated at $T_{ref} = 710\text{K}$ [10].

Parameter (symbol)	Unit	Value
Thermal conductivity (κ_w)	W/(m*K)	29.21
Electrical conductivity (σ_w)	S/m	1.004×10^6

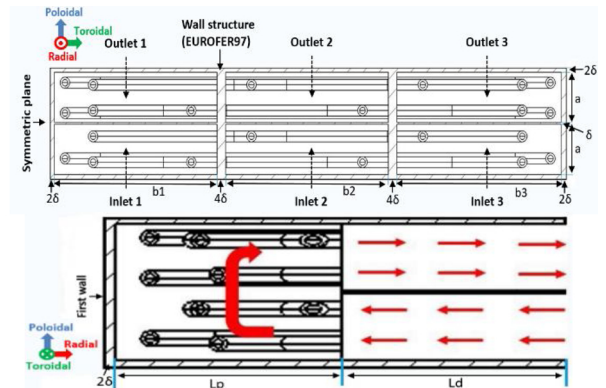


Fig. 3. Computational domain of WCLL blanket module cell [13] in isometric view (left), section view on toroidal-poloidal plane (top right) and section view on radial-poloidal plane (bottom right).

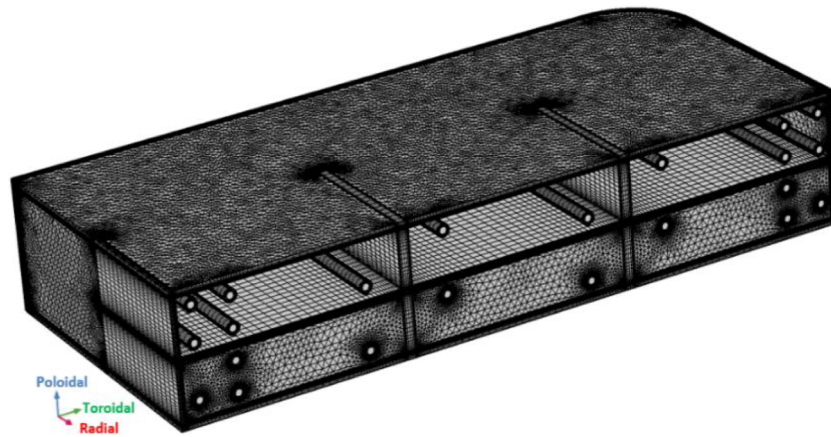


Fig. 4. Example mesh distribution in the computational domain.

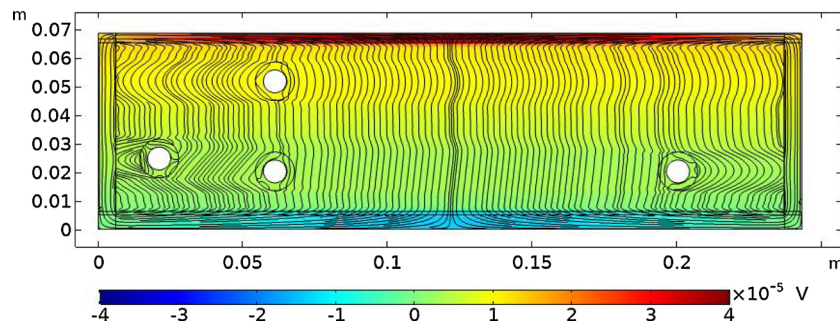


Fig. 5. Electrical potential distribution and current density streamline of fully developed MHD flow on inlet 1 surface.

Table 4

Mesh refinement on boundary layers of inlet 1.

Case	No. of Ele. on boundary layers			Pressure drop (Pa/m)	Maximum velocity (mm/s)
	Hartmann wall ($\delta_{Ha} = \frac{b \cdot \ln(Ha^*)}{Ha}$)	Sidewall ($\delta_{Side} = \frac{b}{Ha^{0.5}}$)	Water pipe wall ($\delta_{WP} = \frac{b}{Ha^{0.5}}$)		
#1	4	5	5	70.279	1.299
#2	5	6	6	50.238	3.528
#3	6	8	8	50.151	3.518
#4	10	10	10	50.151	3.517

*Hartmann number in this study is defined as $Ha = bB_0\sqrt{\sigma/\mu} = 11530$, where the length scale, $b = 0.5 * (\frac{b_1 + b_2 + b_3}{3})$.

Table 5

Mesh refinement on bulk region of breeding zone.

Mesh case	No. of Ele.	Max. Ele. size (mm)	Min. Ele. size (mm)	Max. Ele. growth rate	Max/Avg \bar{U} (mm/s)	Max/Avg \bar{T} (K)	Max \bar{T} on structure /pipe wall (K)
Coarse	2.20 M	21.1	6.34	1.25	24.6/1.21	704/610	704/673
Normal	2.76 M	8.5	4.23	1.2	28.2/0.753	764/630	762/667
Fine	3.23 M	7.5	3.73	1.2	28.9/0.781	763/630	762/667

Table 6

Simulation input conditions.

Parameter (symbol)	Unit	Value
PbLi inlet velocity (u_0)	mm/s	0.178
PbLi inlet temperature (T_0)	°C	325
First wall heat flux (q_0)	kW/m ²	-130
Cooling water temperature (T_{ext})	°C	312
Toroidal magnetic field strength (B_0)	Tesla	4
Nuclear heating power (q_V)	MW/m ³	Eq. (6)

Table 7

Boundary conditions.

Governing equations	Inlet	Outlet	Wall/PbLi interface
Navier-Stokes (\mathbf{u}, p)	\mathbf{u}_0	$p = 0, \nabla \mathbf{u} \cdot \mathbf{n} = 0$	Non-slip
Heat transfer (T)	T_0	$-\mathbf{n} \cdot \kappa \nabla T = q, q = h_{PbLi/CP}(T_{water} - T_{wall})$ at PbLi/CPs	$q = q_0$ at PbLi/first wall; $q = 0$ at other walls and outlet
Electrical potential (θ)	Continuous at PbLi/wall interface;	$\mathbf{n} \cdot \nabla \theta = 0$ at other walls and inlet/outlet	

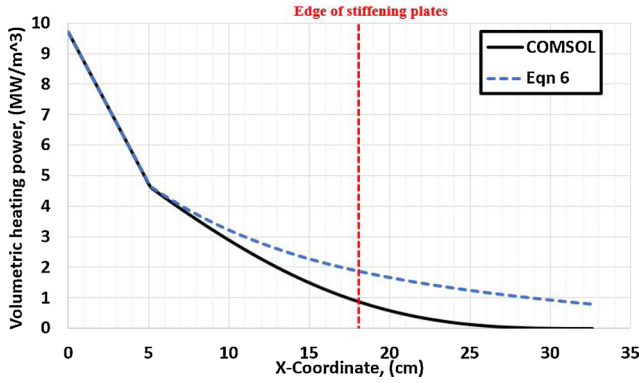


Fig. 6. Volumetric heating power profiles along the radial direction of Eq. (6) [13] and in COMSOL simulation.

$$H(x) = \begin{cases} 1, & x < 0.03 \text{ (m)} \\ 0.5 + 0.9375 \cdot \left(\frac{0.18 - x}{0.15}\right) & , 0.03 \text{ (m)} \leq x \leq L \\ -0.625 \cdot \left(\frac{0.18 - x}{0.15}\right)^3 + 0.1875 \cdot \left(\frac{0.18 - x}{0.15}\right)^5 & \end{cases} \quad (7)$$

3.3. Initial and terminal conditions

Before simulating magneto-convection flows in the WCLL blanket module cell, the temperature distribution with stagnant PbLi flow ($\mathbf{u} = 0$) was firstly calculated (Fig. 19a). Then, the full set of the governing equations were solved using this temperature field combined with zero values of velocity and electrical potential fields as the initial conditions. By monitoring the temporal change of the averaged velocity magnitude (U_{avg}) and temperature (T_{avg}) as plotted in Figs. 7 and 8, the simulations are finally terminated when the change of U_{avg} is stable as well as the dropping rate of T_{avg} is smaller than 0.05 K/s, which corresponds to about 5 % of internal energy loss ($Q_{PbLi} = \iiint \rho C_p \frac{dT}{dt} dV$) in the comparison with the total volumetric heating input power ($Q_v = \iiint q_v dV$). Although the temperature field might still vary slightly with a longer computational time, additional change in thermal energy balance would not alter the main flow feature and heat transfer behaviors.

4. Results and discussion

4.1. Mesh sensitivity study

To evaluate the feasibility of different mesh cases (Table 5), the simulation was firstly conducted with coarse mesh, which was found to be insufficient as it produces improper flow behaviors. As shown in Fig. 9 in which the mass flow rate is calculated on all three inlet and outlet surfaces under three different mesh resolutions, the simulation under coarse mesh delivered a much lower flow rate in the outlet duct 2, which seems contradictory to the design features. Specifically, as illustrated in Fig. 3, aside from the geometrical asymmetric effects of inlet/outlet duct 3, the flow is not expected to deviate into neighboring ducts, and thus the flowrate of each duct’s outlet should be approximately the same. Taking the rounded corner of inlet/outlet duct 3 into account, one would expect to see slightly less outflow in the outlet duct 3 and slightly more outflow in other two ducts to compensate accordingly as demonstrated in the normal and fine mesh cases (Fig. 9). Aside from this discrepancy found in the flowrate, this coarse mesh also used a uniform inlet temperature as the initial condition for the analysis. It turned out that it required a quite significant developing and computational time to reach the termination condition. Further analysis for a normal or a fine mesh uses temperature distributions derived from the stagnation flow as the initial condition as discussed in Section 3.3.

Time evolutions of averaged velocity magnitude (U_{avg}) and temperature (T_{avg}) are plotted in Figs. 7 and 8, respectively, with two spatially averaged domains being applied. These include 1) the entire breeding zone and 2) a y-z slot region (radial-toroidal-poloidal notation is replaced by x-y-z as the coordinated system in this chapter) near the first wall with three times of side-wall boundary layer thickness (δ_{side}), which is illustrated in the blue shaded area in Fig. 10. As the flow evolution approaches the termination time frame, the variation of U_{avg} with respect to time shows a good match qualitatively and quantitatively. Furthermore, the changes in T_{avg} are almost identical in all time frames between normal mesh and fine mesh studies. The good agreements of maximum and spatial averaged velocities and temperature on the entire breeding zone and on few critical components at the final time step are found between normal and fine mesh runs (summarized in Table 5). Specifically, with the mesh refinement from normal mesh study, there are 2.5 % and 3.7 % differences in maximum and spatial averaged velocities, and a negligible difference in temperature on those parts of interest. From all the evidence of comparison in Table 5, as well as Figs. 7, and 8, numerical data obtained from both mesh strategies are shown to be adequate for the present study. The results discussed in the

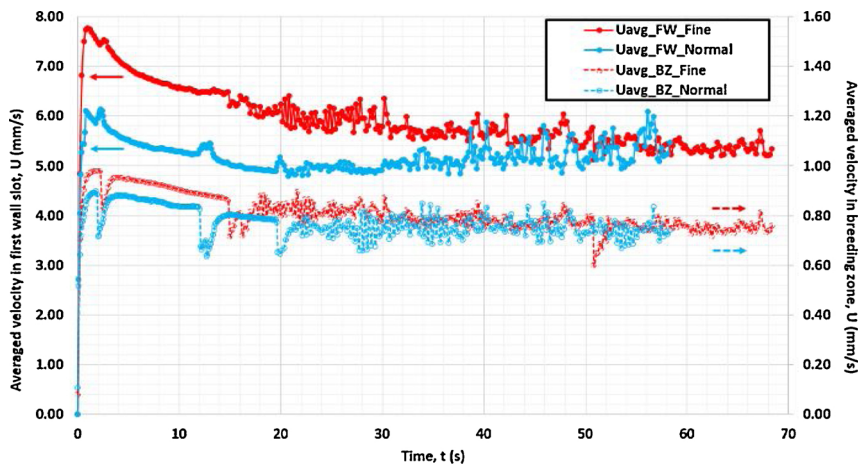


Fig. 7. Spatial averaged velocity magnitude vs. time on normal and fine mesh studies.

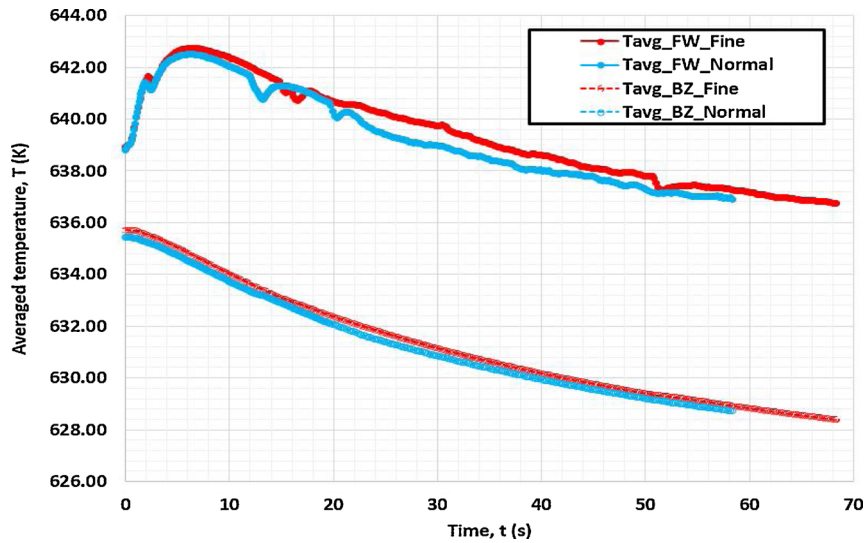


Fig. 8. Spatial averaged temperature vs. time on normal and fine mesh studies.

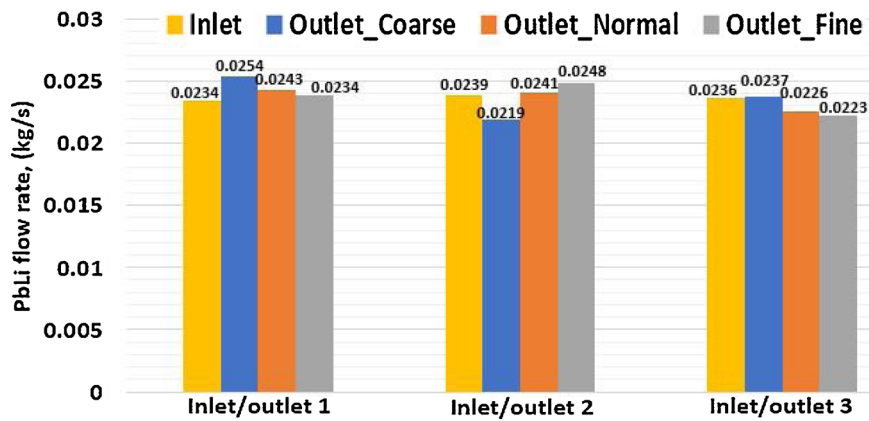


Fig. 9. Flow distribution on three inlet and outlet ducts under three different mesh case studies where the coarse mesh failed to address the physical flow distribution due to a significant discrepancy of flow rate in outlet 2.

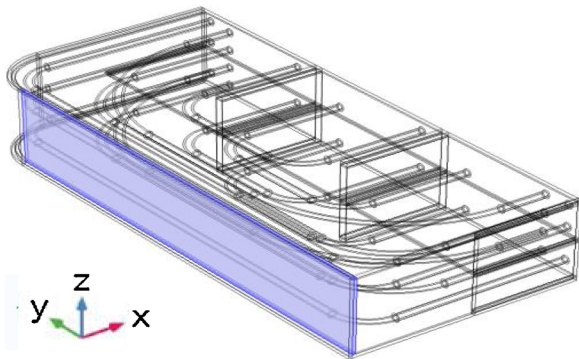


Fig. 10. First wall poloidal-toroidal slot with one boundary layer thickness.

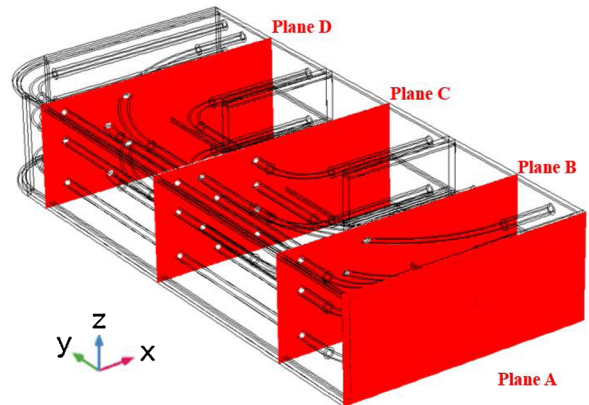


Fig. 11. Locations of four radial-poloidal (x-z) planes (A: $y = 0$; B: $y = 121.5$; C: $y = 346.5$; D: $y = 607.5$ [mm]).

rest of this section are derived from the simulation using the fine mesh and from a flow time of 68 s' simulation (Fig. 11).

4.2. Magneto-convection flow and temperature dynamics in the prototypical WCLL module cell

The simulations were initialized with steep temperature gradients due to the volumetric nuclear heating power, so at the start, the upward flow motion induced by buoyancy force, was generated in the bulk PbLi plenum region, and then evolved into two recirculations with counter-

clockwise through the first wall boundary layer and clockwise through the edge of stiffening plate ($x = 18$ cm) as shown in Fig. 12 at $t = 4$ s. These two counter-rotating flow circulations, with different sizes, occupied the entire space in PbLi plenum region. At the same time, high-speed, laminar flow jets were created due to the strong MHD effects [16,17] near the side-walls (Fig. 14) that are parallel to the applied magnetic field direction. With the buoyancy-driven fluid motion, hot

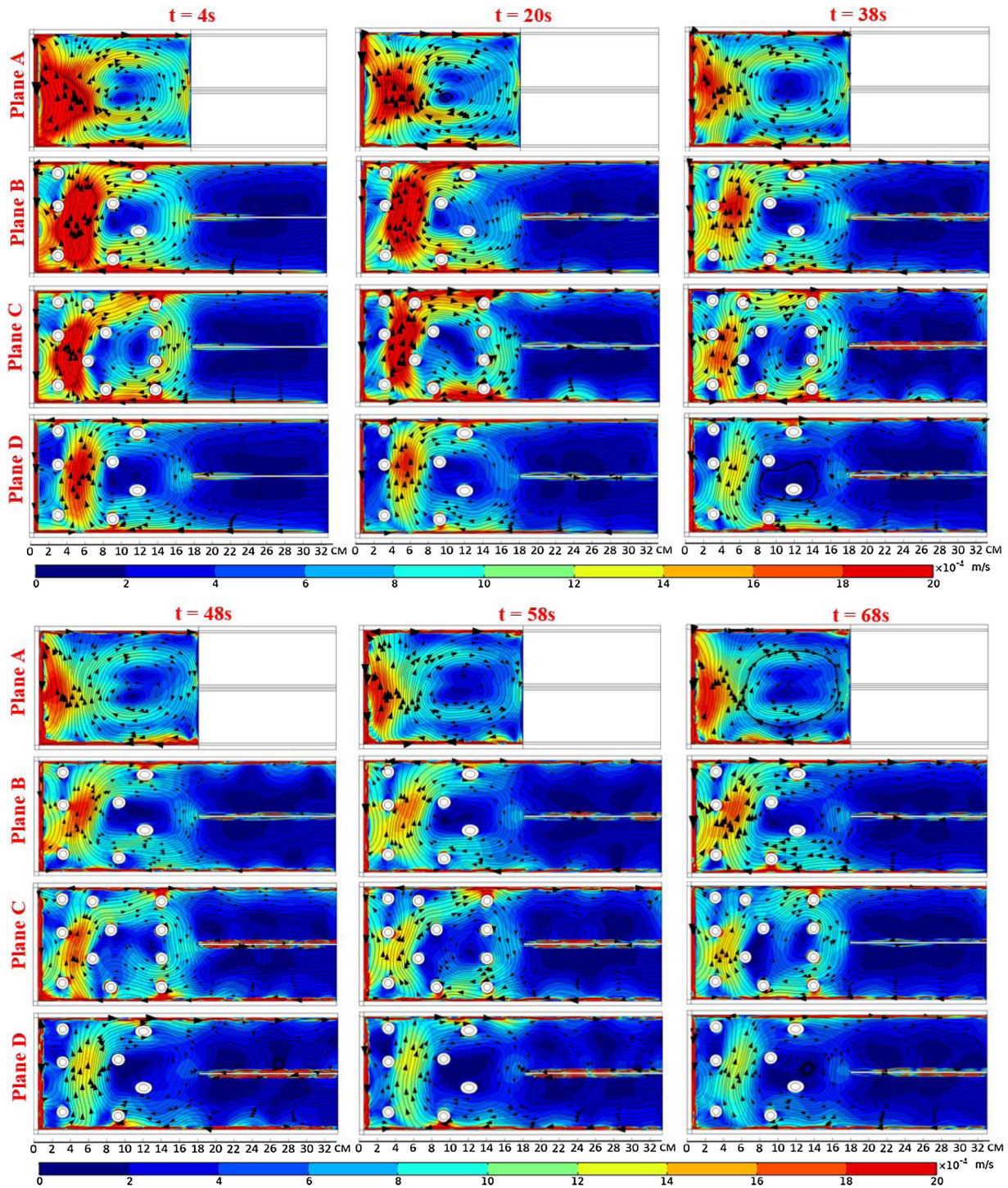


Fig. 12. Surface contour plots of velocity magnitude and streamline of u, w components at plane A-D (Fig. 11) shown from top to bottom, and at different time steps shown from left to right. (Velocity magnitude exceeding 2 mm/s is colored in red).

particles inside the plenum zone either moved up and stayed stratified on the top PbLi/wall interface, or followed the flow path with their thermal energy removed eventually by the first wall heat sink or water-cooling pipes.

When evolved with time, the temperature gradient in the plenum region decreases as can be observed from the temperature profile plots in Fig. 15. As a result, the flow circulations speed became slower at later times as shown in Fig. 12, and their main features appeared still laminar and nearly the same shape that covered the entire flow plenum region.

However, the side-layer jets started to deform into unsteady vortices in all radial-poloidal planes (Fig. 12) since $t = 20 \text{ s}$, leading the flow near the sidewalls changed from a laminar regime to that of a so-called Type I flow instability regime in [18] or unstable regime U1 in [19] (the trend of fluctuation is also demonstrated in Fig. 7). These unsteady flow vortices would travel along the sidewalls and interact with the boundary layers of nearby water pipes as shown in Figs. 12 and 16. However, due to the strong magnetic damping effects, these unsteady flow interactions were weak and localized as the side-wall flow

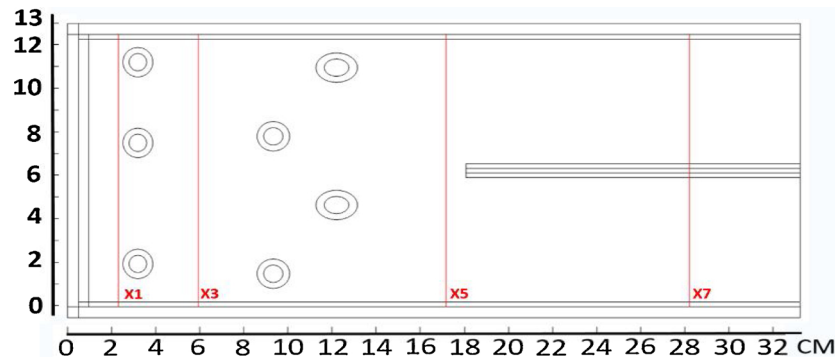


Fig. 13. Location of four reference lines along Z at different x in plane B (X1: x = 23; X3: x = 59; X5: x = 171; X7: x = 281 [mm]).

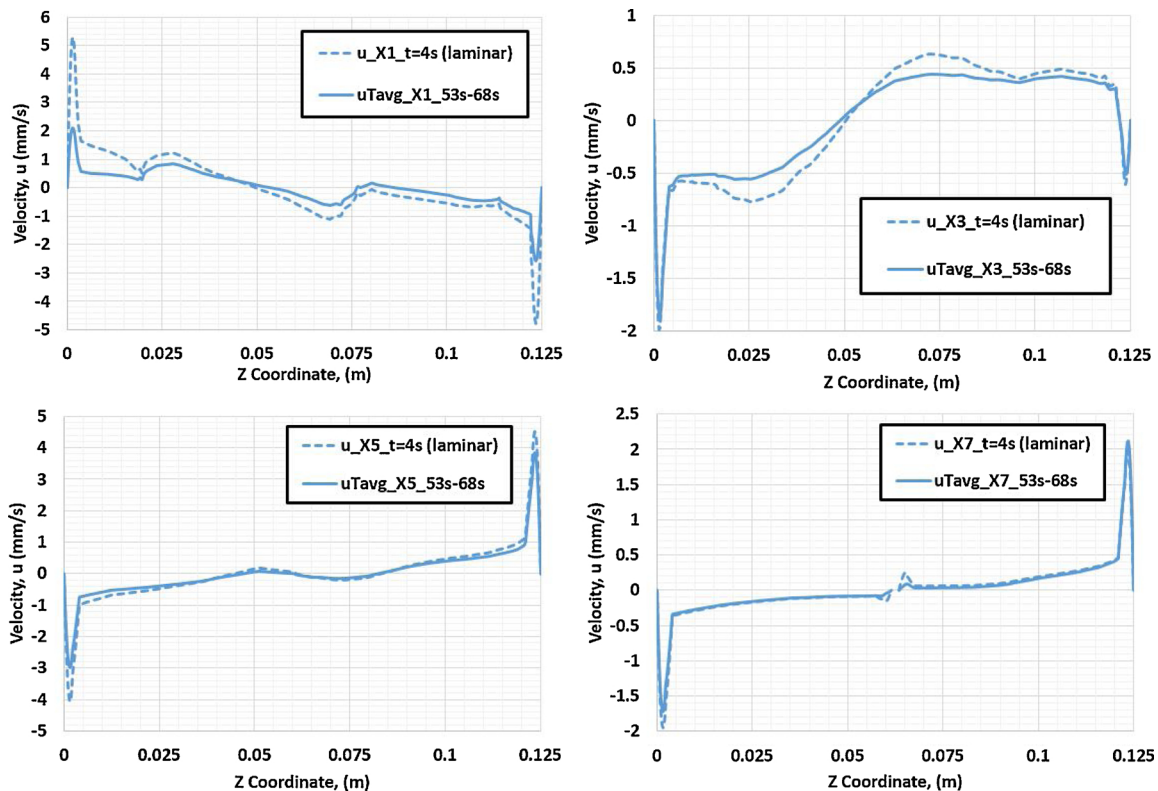


Fig. 14. 1D plot of velocity u component distribution along z direction at different x locations (Fig. 13) in Plane B.

perturbations were confined in the vicinity of the jet region without the growth in space or in strength as illustrated from the dynamics of flow vortices, identified by Q criterion [20] in Fig. 16. Such flow behaviors were also confirmed in the experimental study conducted by Burr et al [18], and Bühler and Horanyi [19]. By the time the simulation was terminated, the change of the temperature field at the entire breeding zone was insignificant when comparing its distribution between 48 s and 68 s in Fig. 15 (< 5 K of temperature reduction in 20 s).

Aside from the minor and negligible changes in the temperature distributions, the bulk flow motion in PbLi plenum region appeared approximately reaching an equilibrium state in the last 15 s of the computational time by comparing the results at t = 68 s with time-averaged results of a time integral from 53 s to 68 s as plotted in Fig. 17. As the velocity distribution with three different time integrals in the last 15 s (plotted in Fig. 18) converged to the same profile, the fluctuations near side-wall boundary layers also reached a statistically steady state (Fig. 19).

4.3. Discussion of the general flow and temperature features of the WCLL unit cell revealed in the simulation

Due to the strong magneto-convection flow motion and the efficient water cooling system, the temperature in the entire domain drops in 40–50 K from the initial temperature distribution (Fig. 18a–b) and leads to no hot areas with the temperature higher than 825 K, which is the material limit of Eurofer 97 steel [21]. However, there are still three spots on the top PbLi/wall interface with a high temperature greater than 723 K, as shown in Fig. 20, that may exceed the corrosion design criterion [22,23].

Not like other types of liquid metal breeding blankets [1], the PbLi flow in WCLL blanket is designed to recirculate in the whole loop for the purpose of tritium breeding and transport without carrying the heat that is generated in the breeding zone. With fusion relevant operational parameters being applied in the present study, the thermal energy removed by PbLi flow is calculated to be 0.21 % of the total heat that is generated in the PbLi region.

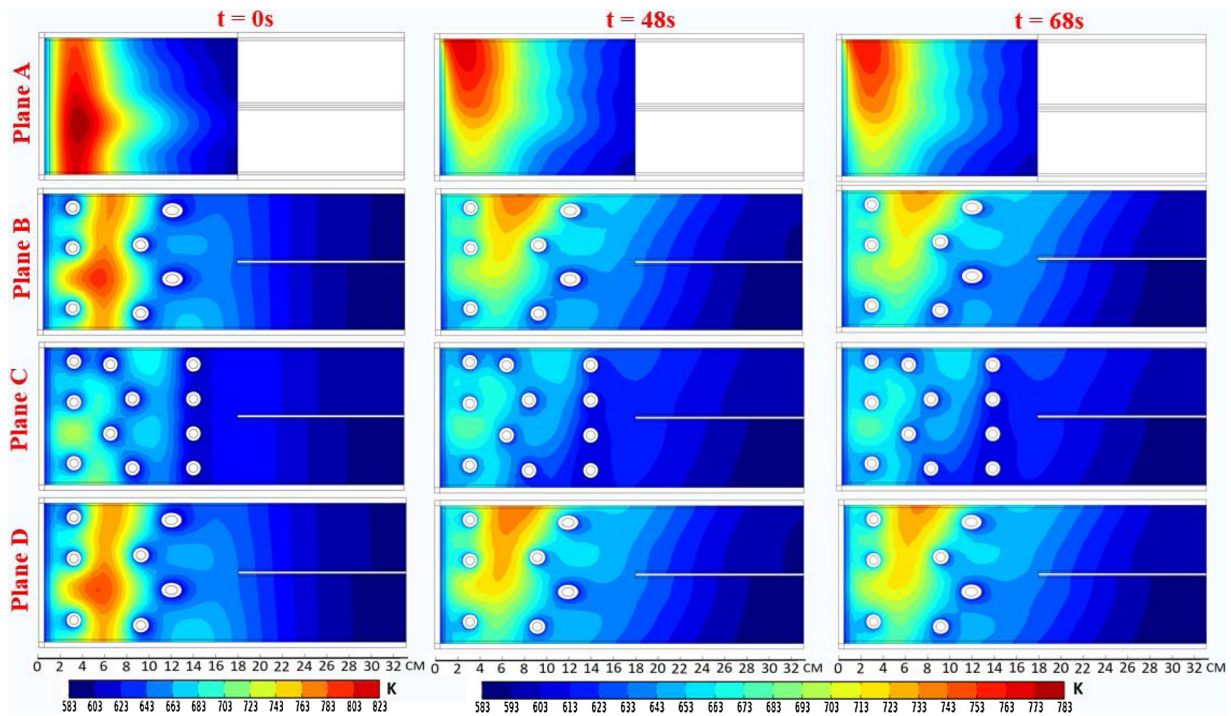


Fig. 15. Surface contour plots of temperature plane A-D shown from top to bottom, and at time $t_0 = 0s$, $t_2 = 48s$, $t_3 = 68s$ shown from left.

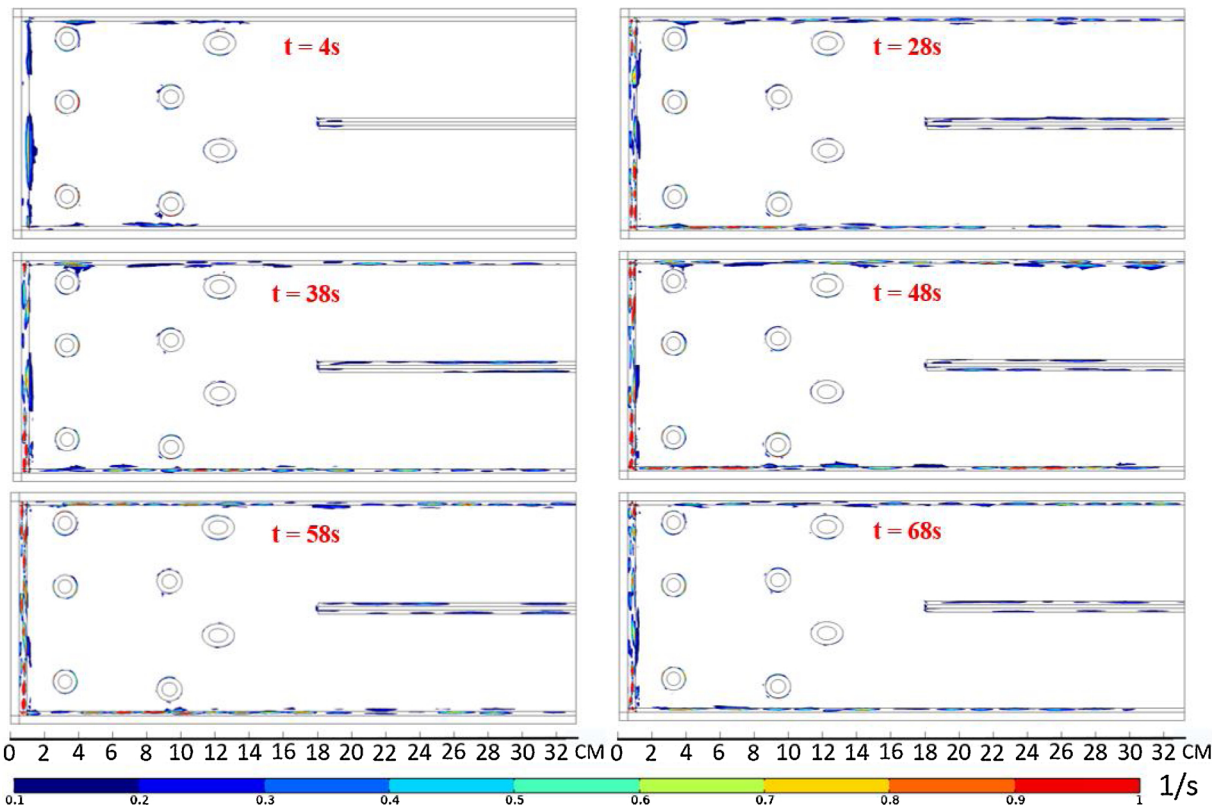


Fig. 16. Surface contour plots of Q variable at plane B at different time steps indicating the flow motions along the side-wall boundary layers.

The bulk velocity and temperature distributions at the final time step along the radial direction (x) are plotted in Fig. 21 with calculation expression: $V_{Bulk} = \frac{\iint V(x,y,z)dydz}{A(x)}$, where V represents either U or T for velocity magnitude and temperature respectively, and $A(x)$ is the integrated area of $y-z$ plane at different x locations. As shown in this

figure, the high flow jet formed in the vicinity of the first wall has the magnitude 70 times larger than the inlet velocity which may lead to a dominant effect on heat and mass transfer. Although the breeding zone is cooled down by the magneto-convection fluid motion, the temperature distribution in the inlet/outlet duct region remains almost the same

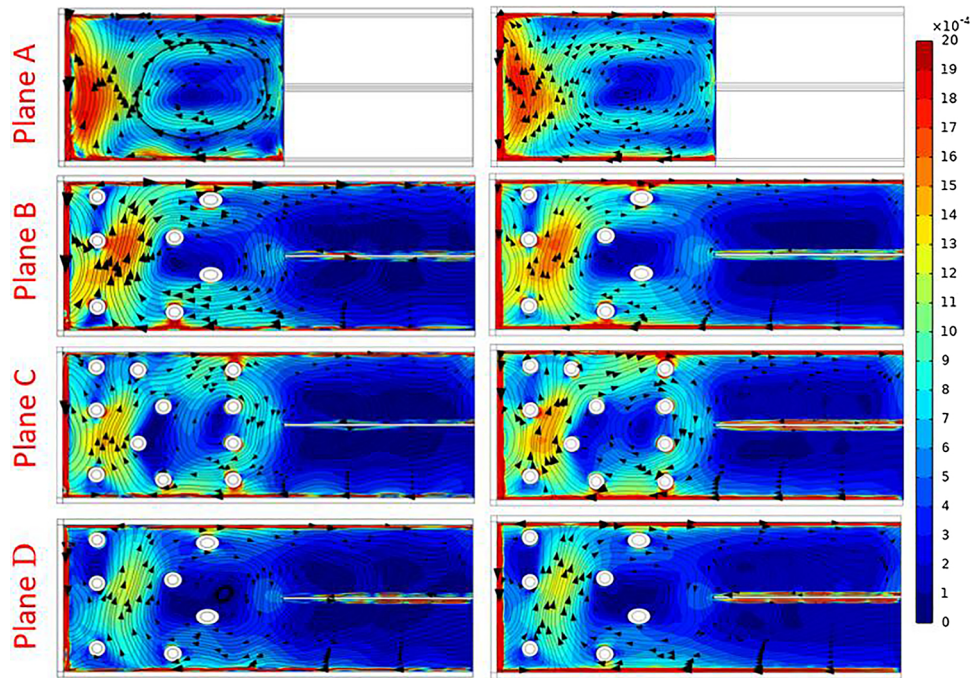


Fig. 17. Surface contour plots of velocity magnitude and streamline of u, w components at plane A-D shown from top to bottom, and at t = 68 s (left) and averaged from t = 53 s to t = 68 s (right). (Velocity magnitude exceeding 2 mm/s is colored in red).

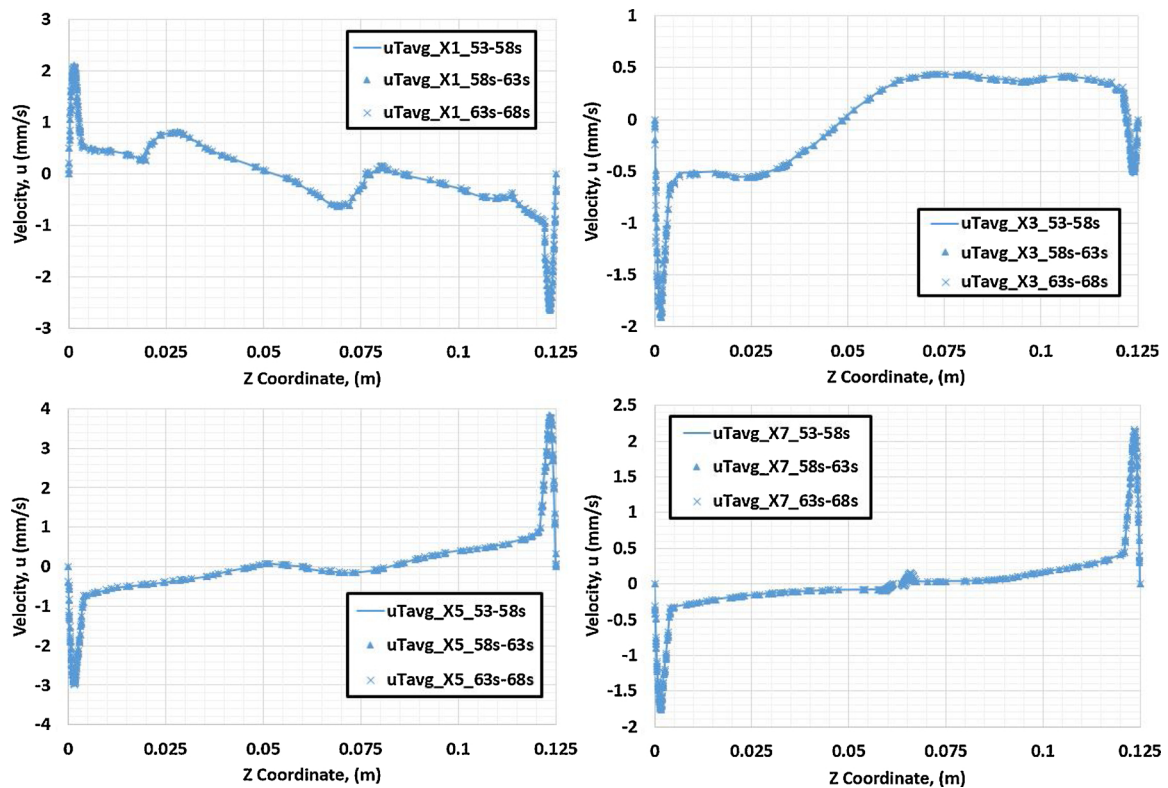


Fig. 18. 1D plots of time-averaged velocity distribution with different time integrals along z direction at different x locations (Fig. 13) in Plane B.

confirming that the bulk counter-rotating circulations mainly circulate in the plenum region. Furthermore, the maximum temperature, with or without the advection effect, appears at the same y-z plane (x = 5 cm) indicating the flow circulations were separated at this particular plane as most of the hot particles traveled upward to the top wall.

4.4. Discussion of COMSOL simulation results

As part of the objective in the evaluation of the modeling capability of COMSOL Multiphysics, several flow features expected to occur in WCLL are captured in this simulation. First of all, similar to the non-isothermal MHD flow recirculation in a rectangular enclosure, a natural

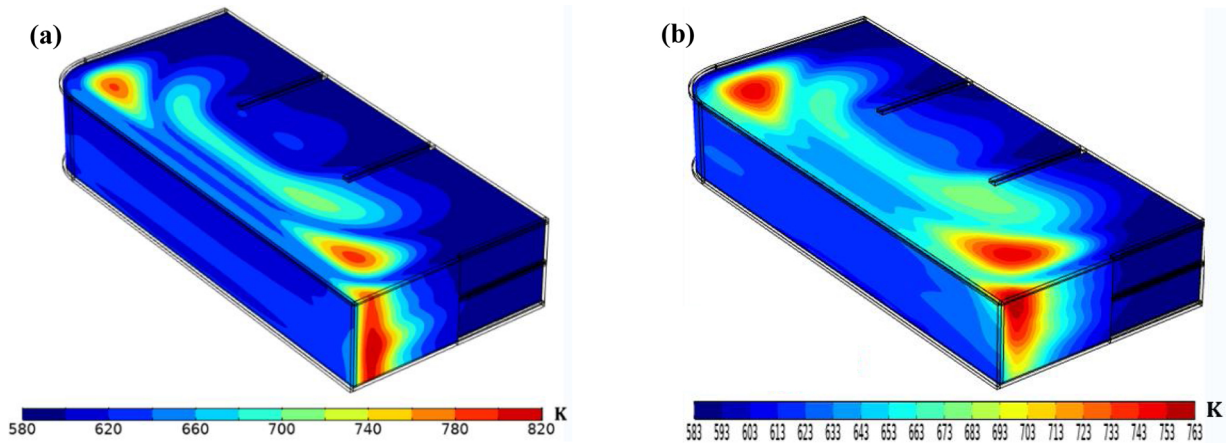


Fig. 19. Temperature distribution on whole WCLL blanket computational domain at $t = 0$ s (a) with PbLi is stagnant and at $t = 68$ s (b) where the simulation is terminated.

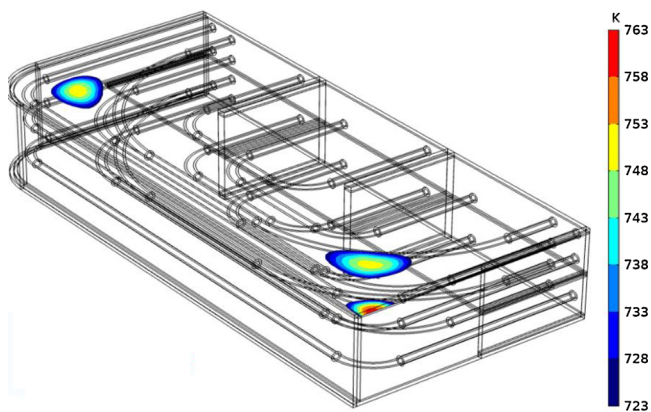


Fig. 20. Hot spot areas on top wall with local temperature greater than 723 K in WCLL.

convection dominated flow motion in the present study was generated in the plenum region as shown in Figs. 12 and 17. Furthermore, because of the non-uniform volumetric heat generation profile, the flow recirculation broke into two counter-rotating circulations separated by

the hottest region, which is comparable to the flow behaviors presented in [24,25]. Besides the flow circulations occupying almost the entire fluid region, the strong MHD effects also created the high velocity boundary layer flow jets, similar to a commonly known MHD side-layer jet in a duct flow with electrically conducting walls as characterized by Hunt [16] and Hunt and Stewartson [17]. In the presence of strong viscous shear forces, which are associated with steep velocity gradients near the side-wall boundary layers, the high-speed jet would break into unsteady vortices. These vortices have been previously observed in simulations performed by Vetcha et al. [26] and the transition from a laminar flow jet to a boundary layer unsteady flow regime has been identified in experiments by Burr et al. [18] and by Bühler and Horanyi [19], although the corresponding formation mechanism at high Hartmann numbers close to the fusion operating condition is still under investigation. Because of the large MHD effect comparing with the inertial effect in this study, those unsteady vortices would stay confined in the vicinity of sidewalls without penetrating into the bulk region of which behavior is similar to the case of secondary instability for higher Reynolds numbers as captured in [26] and [27], and measured in [18] and [19]. In the end, by comparing the flow distribution plots on different x-y planes shown in Fig. 12, the major flow motions are relatively unchanging along the magnetic field direction except for some localized

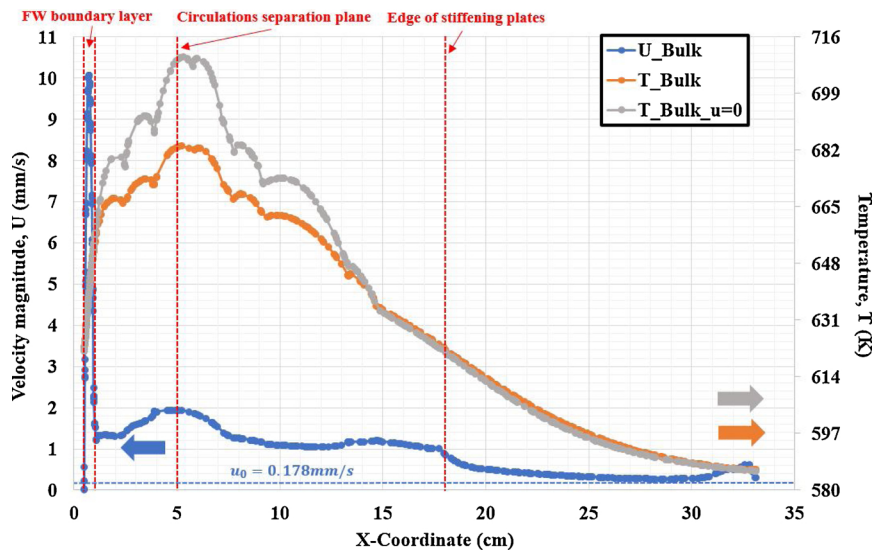


Fig. 21. Time averaged bulk velocity magnitude and temperature distribution along radial direction at $t = 68$ s.

deformations due to geometrical perturbations. This similitude along the magnetic field direction is owed to the tendency of MHD flows when subject to a sufficiently high applied magnetic field to become quasi-two-dimensionality (Q2D) [28].

5. Conclusion

The modeling capability of COMSOL Multiphysics for the study of MHD/heat transfer flows in a complex geometry under fusion relevant conditions is examined by simulating the magneto-convection flow in a prototypical WCLL blanket module cell containing sufficient geometric complexity with the approximately same operational conditions incurred in a DEMO outboard situation. By revealing the MHD flow characteristics that have been demonstrated in previous literature under similar conditions, COMSOL Multiphysics has proven to be capable of simulating the fully coupled MHD/heat transfer equations in a complex geometry with input parameters as stringent as fusion operating conditions.

As the first numerical study of MHD/heat transfer flows in a prototypical WCLL blanket module cell under relevant fusion operating conditions, the magneto-convection flow behaviors and the temperature distribution revealed in the present study would be helpful in the evaluation of the current WCLL breeding blanket designs. Specifically, the flow in the PbLi plenum region, which is of the most interest, is governed by the natural convection effect, leading to two counter-rotation flow circulations that appear to be stable, in spite of weakly interactions with the side-wall unsteady vortices. The temperature distribution, for the first time, was calculated here. Notably, the maximum temperature in the entire computational domain is below the material temperature limit (550 °C); however, corrosion may be an issue as the flow being stratified on the top structure wall where the temperature exceeds the corrosion temperature limit of 475 °C (723 K) in some areas. Furthermore, the thermal energy removed by PbLi flow is calculated to be 0.21 % of the total heat generated in the breeding cell.

CRedit authorship contribution statement

Yi Yan: Methodology, Software, Validation, Formal analysis, Investigation, Data curation, Writing - original draft, Visualization, Project administration. **Alice Ying:** Conceptualization, Methodology, Validation, Investigation, Resources, Writing - review & editing, Supervision, Project administration. **Mohamed Abdou:** Resources, Project administration.

Declaration of Competing Interest

The authors declare that they have no known competing financial interests or personal relationships that could have appeared to influence the work reported in this paper.

Acknowledgements

The CAD model of the WCLL design and input data of the operating parameters provided by Drs. Fabio Cismondi and Alessandro Del Nevo are very much appreciated.

Appendix A. Supplementary data

Supplementary material related to this article can be found, in the online version, at doi:<https://doi.org/10.1016/j.fusengdes.2020.111688>.

References

- [1] M. Abdou, N. Morley, S. Smolentsev, et al., Blanket / first wall challenges and required R & D on the pathway to DEMO, *Fus. Eng. Des.* 100 (2014) 2–43.
- [2] G. Federici, L. Boccaccini, F. Cismondi, et al., An overview of the EU breeding blanket design strategy as an integral part of the DEMO design effort, *Fus. Eng. Des.* 141 (2019) 30–42.
- [3] A. Tassone, A. Del Nevo, P. Arebam, et al., Recent progress in the WCLL breeding blanket design for the DEMO fusion reactor, *IEEE Trans. Plasma Sci.* 46 (5) (2018) 1446–1457.
- [4] A. Del Nevo, E. Martelli, P. Aerna, et al., WCLL breeding blanket design and integration for DEMO 2015: status and perspectives, *Fus. Eng. Des.* 124 (2018) 682–686.
- [5] L. Bühler, C. Mistrangelo, MHD flow and heat transfer in model geometries for WCLL blankets, *Fus. Eng. Des.* 124 (2017) 919–923.
- [6] A. Tassone, G. Caruso, F. Giannetti, et al., MHD mixed convection flow in the WCLL: heat transfer analysis and cooling system optimization, *Fus. Eng. Des.* 146 (2019) 809–813.
- [7] F. Flores, A. Recuero, Magneto-hydrodynamic entrance flow in a channel, *Appl. Sci. Res.* 25 (1972) 403–412.
- [8] E. Martelli, A. Del Nevo, P. Arena, et al., Advancements in DEMO WCLL breeding blanket design and integration, *Int. J. Engery Res.* 42 (2018) 27–52.
- [9] E. Mas de les Valls, et al., Lead-lithium eutectic material database for nuclear fusion technology, *J. Nucl. Mater.* 376 (2008) 353–357.
- [10] K. Mergia, N. Boukos, Structural, thermal, electrical and magnetic properties of Eurofer 97 steel, *J. Nucl. Mater.* 373 (2008) 1–8.
- [11] S. Sahu, R. Bhattacharyay, Validation of COMSOL code for analyzing liquid metal magnetohydrodynamics flow, *Fus. Eng. Des.* 127 (2018) 151–159.
- [12] Y. Yan, Validation of COMSOL multiphysics for magneto-hydro-dynamics (MHD) flows in fusion applications, COMSOL Conference 2017 Boston, October 05 2017, Boston, USA, 2017.
- [13] Private Communication. Information Provided by Fabio Cismondi and Alessandro Del Nevo From Euro-Fusion.
- [14] COMSOL Multiphysics Reference Manual, COMSOL, 2019 Version COMSOL 5.5.
- [15] I. Tosun, *Modeling in Transport Phenomena - a Conceptual Approach*, 2nd edition, Elsevier Science, 2007.
- [16] J.C.R. Hunt, Magneto-hydrodynamic flow in rectangular ducts, *J. Fluid Mech.* 21 (4) (1965) 577–590.
- [17] J.C.R. Hunt, K. Stewartson, Magneto-hydrodynamic flow in rectangular ducts. II, *J. Fluid Mech.* 23 (3) (1965) 563–581.
- [18] U. Burr, L. Barleion, U. Müller, et al., Turbulence transport of momentum and heat in magneto-hydrodynamic rectangular duct flow with strong sidewall jets, *J. Fluid Mech.* 406 (2000) 247–279.
- [19] L. Bühler, S. Horanyi, Measurements of time-dependent liquid-metal magneto-hydrodynamic flows in a flat rectangular duct, *Fus. Eng. Des.* 84 (2009) 518–521.
- [20] J. Jeong, F. Hussain, On the identification of a vortex, *J. Fluid Mech.* 285 (2005) 69–94.
- [21] E. Martelli, G. Caruso, F. Giannetti, et al., Thermo-hydraulic analysis of EU DEMO WCLL breeding blanket, *Fus. Eng. Des.* 130 (2018) 48–55.
- [22] P. Tortorelli, J. DeVan, Corrosion of ferrous alloys exposed to thermally convective Pb-17 at % Li, *L. Nucl. Mater.* 131–143 (1986) 592–598.
- [23] J. Sannier, M. Broc, T. Flament, et al., Corrosion of austenitic and martensitic stainless steels in flowing Pb17Li alloy, *Fus. Eng. Des.* 14 (1991) 299–307.
- [24] I.E. Sarris, S.C. Kakarantza, et al., MHD natural convection in a laterally and volumetrically heated square cavity, *Int. J. Heat Mass Transf.* 48 (2005) 3443–3453.
- [25] M. Obayedullah, M.M.K. Chowdhury, MHD natural convection in a rectangular cavity having internal energy sources with non-uniformly heated bottom wall, *Procedia Eng.* 56 (2013) 76–81.
- [26] N. Vetcha, S. Smolentsev, et al., Study of instabilities and quasi-two-dimensional turbulence in volumetrically heated magneto-hydrodynamic flows in a vertical rectangular duct, *Phys. Fluid* 25 (2013) 024102.
- [27] M. Kinet, B. Kneapen, S. Molokiv, Instability and transition in magneto-hydrodynamics flows in ducts with electrically conducting walls, *Phys. Rev. Lett.* 103 (2009) 154501.
- [28] P.A. Davidson, *An Introduction to Magneto-hydrodynamics*, Cambridge University Press, 2001.